1-6-2015

An Experimental and Theoretical Study of the Electronic Spectrum of the HBCl Free Radical

Mohammed A. Gharaibeh
University of Jordan, Jordan

Ramya Nagarajan
University of Kentucky

Dennis J. Clouthier
University of Kentucky, dclaser@uky.edu

Riccardo Tarroni
Università di Bologna, Italy

An experimental and theoretical study of the electronic spectrum of the HBCl free radical

Mohammed A. Gharaibeh,[1] Ramya Nagarajan,[2] Dennis J. Clouthier,[2,a)] and Riccardo Tarroni[3]

[1]*Department of Chemistry, The University of Jordan, Amman 11942, Jordan*
[2]*Department of Chemistry, University of Kentucky, Lexington, Kentucky 40506-0055, USA*
[3]*Dipartimento di Chimica Industriale "Toso Montanari," Università di Bologna, Viale Risorgimento 4, 40136 Bologna, Italy*

(Received 22 October 2014; accepted 9 December 2014; published online 6 January 2015)

Following our previous discovery of the spectra of the HBX (X = F, Cl, and Br) free radicals [S.-G. He, F. X. Sunahori, and D. J. Clouthier, J. Am. Chem. Soc. **127**, 10814 (2005)], the $\tilde{A}^2A''\Pi - \tilde{X}^2A'$ band systems of the HBCl and DBCl free radicals have been studied in detail. The radicals have been prepared in a pulsed electric discharge jet using a precursor mixture of BCl_3 and H_2 or D_2 in high pressure argon. Laser-induced fluorescence (LIF) and single vibronic level emission spectra have been recorded to map out the ground and excited state vibrational energy levels. The band system involves a linear-bent transition between the two Renner-Teller components of what would be a $^2\Pi$ electronic state at linearity. We have used high level *ab initio* theory to calculate the ground and excited state potential energy surfaces and have determined the vibronic energy levels variationally. The theory results were used to assign the LIF spectra which involve transitions from the ground state zero-point level to high vibrational levels of the excited state. The correspondence between theory and experiment, including the transition frequencies, upper state band symmetries, and H, B, and Cl isotope shifts, was used to validate the assignments. © *2015 AIP Publishing LLC.* [http://dx.doi.org/10.1063/1.4904892]

I. INTRODUCTION

Boron carbide is a p-type semiconducting material whose hardness, very high melting point, inertness to chemical attack, and excellent thermal and electrical characteristics make it attractive for semiconductor and coating applications. Deposition of thin layers of boron carbide is primarily accomplished by chemical vapor deposition (CVD) using BCl_3–CH_4–H_2 precursor mixtures although a variety of other boron sources (BBr_3, B_2H_6, $B(CH_3)_3$, etc.) have also been shown to be useful.[1] Boron nitride, the hardest boron-containing compound known, is similarly produced by CVD with BCl_3–NH_3–H_2 gas mixtures.[2]

Despite intensive research into methods of producing boron carbide and boron nitride films and coatings, much remains to be learned about the precise mechanisms of such processes. In 2001, Sezer and Brand[1] concluded that "It was evident from this review that extensive research still remains to be done on the modeling of CVD boron carbides." For example, although *in situ* FTIR studies have identified $BHCl_2$ as an intermediate in high temperature reactions of BCl_3 and hydrogen both in the gas phase and at the surface of a tungsten filament, the elementary reactions are still unclear.[3–5] *Ab initio* methods have been used to predict the thermochemistry[6] and reaction paths[7] of the various intermediates in the BH_mCl_n system and similar calculations on the thermodynamics of molecules in the B–N–Cl–H system have been reported.[8] Harris *et al.*[9] have used the *ab initio* data and transition state and Rice-Ramsperger-Kassel-Marcus (RRKM) theory to calculate rate constants for the thermal decomposition of BCl_3/H_2 gas mixtures which led to a suggested reaction mechanism involving 31 elementary steps. The boron containing free radicals BCl, BCl_2, BH, BH_2, and HBCl were predicted to have substantial gas phase concentrations at various reaction temperatures.

In 2005, we reported the first observation of the HBX (X = F, Cl, and Br) free radicals,[10] reactive species which may play an important role in CVD and etching processes involving hydrogen and boron trihalide precursors. Using laser-induced fluorescence (LIF) methods, we detected these radicals in the products of an electric discharge through BX_3/H_2/Ar mixtures at the exit of a pulsed molecular beam valve. The supersonically cooled species were identified by the characteristic ground state vibrational frequencies and subband splittings in single vibronic level emission spectra. Since the band systems involve a linear-bent transition between the two Renner-Teller components of what would be a $^2\Pi$ state at linearity, the analysis of the LIF spectra is challenging. We have recently[11] used a combination of *ab initio* theory and variational methods to predict the ground and excited state vibrational levels and isotope effects for HBF, which facilitated a detailed study[12] of the $\tilde{A} - \tilde{X}$ band systems of HBF and DBF. In the present work, we have used a similar blend of theoretical and experimental methods to understand the $\tilde{A}^2A''\Pi - \tilde{X}^2A'$ band systems of the HBCl and DBCl free radicals.

a)Author to whom correspondence should be addressed. Electronic mail: dclaser@uky.edu.

II. EXPERIMENT

The HBCl and DBCl free radicals were produced in a discharge free jet expansion[13] using precursor mixtures of 1% BCl_3 and 5% H_2 (or D_2) in high pressure argon. The gas mixture was injected at a pressure of 40 psi through the 0.8 mm orifice of a pulsed molecular beam valve (General Valve, Series 9) into the vacuum chamber. After a short time delay, a pulsed electric discharge was struck between a pair of ring electrodes mounted in a cylindrical Delrin flow channel attached to the exit to the valve, fragmenting the precursors and producing HBCl by secondary reactions. The radicals were cooled to low rotational temperatures (~10 K) by collisions downstream of the discharge. A 1.0 cm reheat tube[14] was attached to the exit of the discharge flow channel to increase the number of collisions which both enhanced the production of the radicals and suppressed the background glow from electronically excited argon atoms.

Low-resolution LIF spectra were recorded by exciting the jet-cooled radicals with the collimated beam of a pulsed tunable dye laser (Lumonics HD-500, linewidth 0.1 cm^{-1}) and imaging the resulting fluorescence signals onto the photocathode of a high gain photomultiplier (EMI 9816QB). The signals were sampled with a gated integrator and recorded with LABVIEW-based data acquisition software. The spectra were calibrated with optogalvanic lines from neon- and argon-filled hollow cathode lamps to an accuracy of ~0.1 cm^{-1}.

The LIF spectra were complicated by overlapping bands of the various HBCl isotopologues and fluorescence from various impurity species produced in the electric discharge. To circumvent these problems, we used the LIF synchronous scanning (sync-scan) technique described previously.[15] In this method, the fluorescence is dispersed by a scanning monochromator which is fixed on a prominent emission band of the isotopologue(s) of interest. The excitation laser and the monochromator are scanning synchronously under computer control so that the resulting spectrum exhibits only those transitions that emit down to the chosen level, focusing on the spectrum of a subset of the molecular isotopologues and minimizing impurity emission. For example, we were able to obtain LIF spectra of $H^{11}BCl$ free of $H^{10}BCl$ bands using this technique.

Single vibronic level (SVL) emission spectra were obtained by laser excitation of the intensity maxima of the stronger bands observed in the LIF sync-scan spectra. The resulting fluorescence was focused onto the entrance slit of a 0.5 m scanning monochromator (SPEX 500M) and the emission was detected with a cooled, red-sensitive photomultiplier (RCA C31034A), amplified by a factor of ~1000, processed with a gated integrator, and then recorded digitally. The spectra were calibrated with emission lines from an argon discharge lamp to an estimated accuracy of ±1 cm^{-1}. The monochromator was equipped with a 1200 line/mm grating blazed at 750 nm and spectra were recorded with a bandpass of 0.6-0.8 nm, depending on the strength of the fluorescence.

III. THEORETICAL CALCULATIONS

A. Preliminary *ab initio* studies

As a preliminary to the calculation of the HBCl potential energy surfaces, we have used density functional theory [B3LYP] and the coupled-cluster singles and doubles with triple excitations included perturbatively [CCSD(T)] method to predict the properties of the ground and excited states using the Gaussian 03 program package.[16] Dunning's correlation-consistent triple-zeta basis set augmented by diffuse functions (aug-cc-pVTZ)[17] was employed for both studies. Ground state HBCl has the electron configuration

$$[\text{core}](6a')^2(7a')^2(8a')^2(2a'')^2(9a')^2(10a')^1(3a'')^0\tilde{X}^2A',$$

where $2a''$ is a BCl out-of-plane B bonding orbital, $9a'$ is a combination of H(1s), B($2p_y$), and Cl($3p_y$) orbitals which is primarily BH bonding, and $10a'$ and $3a''$ are the in- and out-of-plane BCl π antibonding orbitals. The $3a''$ LUMO is primarily an out-of-plane $2p_z$ orbital on the boron atom. Promotion of an electron from the $10a'$ HOMO to the $3a''$ LUMO yields the first electronic excited state which has a linear geometry and is symbolized[18] as $\tilde{A}^2A''\Pi$.

Both the B3LYP and CCSD(T) methods gave similar results, with a bent ground state ($\theta = 123°$) and a linear excited state whose equilibrium bond lengths are 0.02–0.03 Å shorter than the ground state. The difference in the electronic energies of the two states is calculated to be very low (5500–5600 cm^{-1}) as is typical for linear-bent transitions between the two Renner-Teller components of what would be a $^2\Pi$ state at linearity.[19–21] A summary of the theoretical results is given in Table I where the vibrational numbering is defined in standard notation as ν_1 = BH stretch, ν_2 = bend, and ν_3 = BCl stretch.

TABLE I. *Ab initio* predictions of the spectroscopic parameters of the ground and first excited states of $H^{11}B^{35}Cl$ and $D^{11}B^{35}Cl$. All quantities are in cm^{-1} except the geometric parameters.

	$H^{11}B^{35}Cl$	$D^{11}B^{35}Cl$
	$\tilde{X}^2A'$	
ω_1	2641 (2639)[a]	1951 (1949)
ω_2	842 (833)	652 (645)
ω_3	909 (890)	872 (855)
A	20.003 (20.267)	11.633 (11.633)
B	0.5850 (0.5870)	0.5141 (0.5157)
C	0.5683 (0.5705)	0.4923 (0.4941)
r_{HB} (Å)	1.1910 (1.1877)	
r_{BCl} (Å)	1.7236 (1.7202)	
θ_{HBCl} (deg)	123.34 (123.64)	
	$\tilde{A}^2A''\Pi$	
ω_1	2861 (2870)	2133 (2138)
ω_2	682 (680)	532 (531)
ω_3	926 (917)	888 (880)
T_e	6208 (5522)	6208 (5522)
T_0	6247 (5575)	6247 (5572)
B	0.5647 (0.5680)	0.4745 (0.4772)
r_{HB} (Å)	1.1674 (1.1639)	
r_{BCl} (Å)	1.6901 (1.6853)	
θ_{HBCl} (deg)	180.0	

[a]The first numbers are from CCSD(T) theory and those in parentheses are from B3LYP theory, both using an aug-cc-pVTZ basis set.

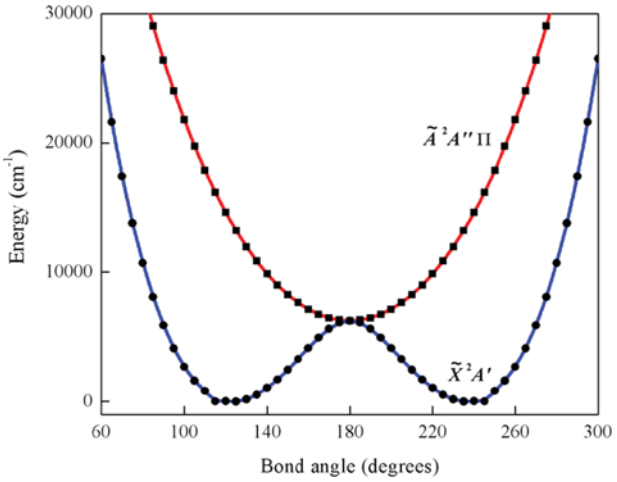

FIG. 1. Potential energy curves along the bond angle coordinate for the $\tilde{X}^2A'$ and $\tilde{A}^2A''\Pi$ states of HBCl. The bond lengths were fixed at their ground state equilibrium values of r_{BH} = 1.7162 Å and r_{BCl} = 1.1897 Å.

B. Calculation of the potential energy surfaces

All single point energy calculations were performed with the CFOUR suite of quantum chemistry programs.[22] Complementary computations of the spin-orbit operator matrix elements were undertaken and performed with the Molpro 2010 code.[23] Single point energies of the bent $\tilde{X}^2A'$ ground state and the linear $\tilde{A}^2A''\Pi$ first excited state were calculated at the CCSD(T) level of theory[24] with the aug-cc-pVQZ basis set (aug-cc-pV(Q + d)Z for chlorine),[25] using unrestricted Hartree-Fock (UHF) wavefunctions with the proper symmetry as references. Only the valence electrons were correlated. The geometries of the single point calculations were carefully chosen in order to properly map the potential energy surfaces (PESs) of the ground and of the excited states for energies up to 20 000 cm^{-1} above their respective minima. The geometries were in the ranges $2.7 \le r_{BCl} \le 4.3$ bohrs and $1.7 \le r_{BH} \le 3.3$ bohrs for the stretching coordinates (both states) and $70 \le \theta_{HBCl} \le 180$ ($\tilde{X}^2A'$ state, 1012 points), $100 \le \theta_{HBCl} \le 180$ ($\tilde{A}^2A''$ state, 633 points). Potential energy curves as a function of bond angle for fixed bond lengths, illustrating the nature of the relevant electronic states, are shown in Fig. 1.

The energies of the two states were fitted using the SURFIT program,[26] which has the advantage of being able to provide second order perturbative estimates of the vibrational frequencies for comparison with experiment, giving an immediate check of the overall quality of the theoretical surfaces. The fitting was done using symmetry restricted polynomial functions with the general form

$$V^{\eta}(q_1, q_2, q_3) = \sum_{ijk} c_{ijk}^{\eta} (q_1 - q_1^{ref,\eta})^i (q_2 - q_2^{ref,\eta})^j (q_3 - q_3^{ref,\eta})^k, \tag{1}$$

where η refers to the specific electronic state, $q_1 = r_{BCl}$ stretching, $q_2 = r_{BH}$ stretching, and $q_3 = \theta_{HBCl}$ bending, and $q_1^{ref,\eta}$, $q_2^{ref,\eta}$, and $q_3^{ref,\eta}$ defines the reference geometry of the ηth state. Symmetry restrictions constrain k to be even for the $\tilde{A}^2A''$ state. The two PESs have been expanded at their computed equilibrium geometries and the fitting coefficients c_{ijk}^{η} are presented as supplementary material.[27] The root mean square deviation (RMSD) of the least squares fitting was 3.9 cm^{-1} and 2.5 cm^{-1} for the $\tilde{X}^2A'$ and $\tilde{A}^2A''$ states, respectively. The degeneracy of the two surfaces at linearity was imposed by simply including 56 linear geometries in the fitting of the ground state coefficients. This procedure was simpler than that adopted for HBF;[11] nevertheless, it was able to recover surfaces which are nearly degenerate for linear geometries, with differences of the same order of magnitude of the RMSDs of the fittings. These tiny differences proved to be irrelevant in the subsequent variational calculation of the rovibronic energy levels. From the fitted surfaces, the barrier

TABLE II. Calculated low-lying $\tilde{X}^2A'$ state vibrational energy levels ($N_{Ka,Kc} = 0_{0,0}$) of the various HBCl isotopologues (in cm^{-1}).

(v_1, v_2, v_3)	$H^{11}B^{35}Cl$	$H^{11}B^{37}Cl$	$H^{10}B^{35}Cl$	$H^{10}B^{37}Cl$	$D^{11}B^{35}Cl$	$D^{11}B^{37}Cl$	$D^{10}B^{35}Cl$	$D^{10}B^{37}Cl$
(0,1,0)	835.2	831.3	845.9	843.0	646.6	645.4	651.7	650.5
(0,0,1)	894.8	892.6	919.6	916.6	863.8	858.6	893.7	888.7
(0,2,0)	1666.3	1658.2	1688.2	1682.5	1289.5	1287.3	1299.9	1297.6
(0,1,1)	1720.7	1715.5	1753.7	1748.2	1502.6	1496.2	1536.8	1530.7
(0,0,2)	1775.9	1770.9	1826.4	1820.0	1715.6	1705.4	1773.0	1763.4
(0,3,0)	2492.9	2480.3	2526.4	2518.0	1928.3	1925.2	1944.2	1941.0
(1,0,0)	2537.8	2533.8	2549.9	2549.8	1899.4	1899.2	1916.7	1916.5
(0,2,1)	2543.8	2539.7	2583.3	2575.5	2137.9	2130.4	2176.6	2169.4
(0,1,2)	2591.8	2584.5	2649.1	2640.4	2347.3	2335.9	2408.8	2397.9
(0,0,3)	2644.5	2636.3	2721.1	2711.1	2556.5	2541.7	2640.6	2559.0
(0,4,0)	3314.3	3296.8	3359.5	3349.1	2562.7	2558.9	2584.4	2580.5
(0,3,1)	3356.0	3348.2	3408.2	3398.9	2766.6	2759.2	2811.4	2803.5
(1,1,0)	3366.4	3360.1	3382.2	3378.6	2538.4	2536.8	2560.5	2559.0
(0,2,2)	3401.4	3392.8	3461.6	3452.3	2975.7	2963.1	3041.3	3029.2
(1,0,1)	3431.0	3425.1	3476.2	3470.7	2772.0	2765.5	2819.9	2814.1
(0,1,3)	3454.2	3446.3	3533.8	3521.7	3181.8	3164.7	3269.5	3254.0
(0,0,4)	3501.9	3490.0	3604.5	3590.7	3386.7	3367.1	3497.2	3478.4
(0,5,0)	4129.8	4107.0	4183.8	4174.1	3193.4	3189.0	3221.1	3216.6
(1,2,0)	...	...	...	...	3171.8	3169.9	3199.0	3196.3

TABLE III. Calculated $\tilde{A}^2A''$ state vibronic levels ($N = K_a$), relative to the lowest vibration-rotation level of the electronic ground state of the HBCl isotopologues (in cm^{-1}).

(v_1, v_2, v_3)	$H^{11}B^{35}Cl$	$H^{11}B^{37}Cl$	$H^{10}B^{35}Cl$	$H^{10}B^{37}Cl$	$D^{11}B^{35}Cl$	$D^{11}B^{37}Cl$	$D^{10}B^{35}Cl$	$D^{10}B^{37}Cl$
(0,1,0)Σ	7 114.7	7 114.2	7 126.4	7 125.9	6 898.5	6 897.9	6 912.8	6 912.2
(0,2,0)Π	7 672.7	7 667.6	7 703.4	7 692.8	7 363.6	7 349.8	7 394.9	7 388.4
(0,3,0)Σ	8 460.3	8 459.3	8 485.8	8 484.9	7 959.5	7 958.1	7 993.4	7 992.0
(0,4,0)Π	9 103.3	9 101.7	9 139.5	9 136.3	8 462.8	8 451.9	8 527.9	8 526.0
(0,5,0)Σ	9 801.0	9 799.7	9 840.7	9 839.4	9 023.4	9 021.1	9 078.3	9 075.9
(0,6,0)Π	10 397.3	10 394.1	10 460.9	10 459.7	9 528.5	9 534.7	9 615.9	9 614.8
(0,7,0)Σ	11 136.2	11 134.4	11 189.9	11 188.1	10 088.7	10 085.3	10 165.6	10 162.0
(0,8,0)Π	11 795.5	11 793.5	11 855.1	11 853.0	10 621.6	10 610.5	10 705.9	10 702.9
(0,9,0)Σ	12 464.7	12 462.5	12 531.0	12 528.8	11 154.1	11 149.6	11 253.7	11 248.9
(0,10,0)Π	13 104.7	13 102.9	13 177.3	13 172.8	11 672.4	11 666.0	11 788.0	11 780.5
(0,11,0)Σ	13 784.2	13 781.6	13 876.2	13 873.7	12 218.7	12 213.0	12 341.4	12 335.3
(0,12,0)Π	14 441.2	14 438.4	14 530.5	14 526.1	12 744.0	12 736.3	12 887.4	12 878.8
(0,13,0)Σ	15 110.7	15 107.0	15 204.1	15 200.8	13 281.6	13 274.6	13 427.8	13 420.3
(0,14,0)Π	15 764.0	15 762.6	15 869.7	15 863.9	13 803.8	13 793.9	13 964.7	13 954.3
(0,15,0)Σ	16 416.2	16 412.2	16 525.3	16 521.5	14 342.0	14 333.7	14 512.0	14 503.1
(0,16,0)Π	17 067.4	17 064.5	17 187.1	17 184.5	14 870.8	14 860.3	15 042.9	15 033.1
(0,17,0)Σ	17 715.3	17 710.6	17 838.5	17 834.1	15 399.4	15 389.8	15 593.2	15 583.0
(0,18,0)Π	18 358.0	18 356.5	18 495.9	18 488.9	15 924.3	15 913.0	16 127.5	16 117.8
(0,19,0)Σ	19 006.3	19 001.9	19 143.1	19 138.1	16 453.1	16 442.2	16 670.9	16 659.3
(0,20,0)Π	19 647.3	19 640.3	19 790.7	19 785.1	16 989.4	16 981.2	17 209.2	17 199.2
(0,21,0)Σ	20 288.6	20 283.3	20 438.5	20 433.0	17 502.8	17 490.5	17 744.4	17 731.4
(0,22,0)Π	20 931.5	20 925.5	21 083.1	21 077.2	18 035.9	18 027.3	18 281.6	18 266.0
(0,1,1)Σ	8 031.7	8 024.9	8 072.0	8 065.5	7 772.9	7 766.3	7 808.5	7 802.1
(0,2,1)Π	8 544.9	8 543.4	8 616.9	8 605.3	8 221.9	8 216.6	8 264.7	8 249.5
(0,3,1)Σ	9 372.2	9 365.1	9 425.8	9 418.9	8 824.1	8 816.9	8 877.4	8 870.5
(0,4,1)Π	10 006.0	9 998.6	10 070.5	10 064.4	9 324.1	9 313.8	9 387.2	9 372.5
(0,5,1)Σ	10 707.8	10 700.3	10 775.0	10 767.7	9 878.3	9 870.4	9 950.6	9 943.0
(0,6,1)Π	11 362.2	11 355.2	11 435.3	11 427.8	10 408.5	10 394.1	10 484.9	10 459.4
(0,7,1)Σ	12 037.9	12 029.9	12 118.4	12 110.7	10 933.7	10 925.0	11 026.2	11 017.7
(0,8,1)Π	12 691.5	12 683.3	12 778.9	12 770.7	11 492.6	11 490.7	11 582.7	11 563.1
(0,9,1)Σ	13 361.4	13 353.0	13 454.9	13 446.8	11 989.2	11 979.5	12 102.5	12 093.0
(0,10,1)Π	14 019.9	14 012.6	14 122.6	14 118.5	12 506.8	12 493.1	12 626.0	12 609.8
(0,11,1)Σ	14 677.1	14 668.5	14 792.5	14 784.6	13 043.8	13 033.2	13 178.5	13 168.0
(0,12,1)Π	15 330.6	15 322.1	15 449.6	15 439.3	13 569.4	13 556.1	13 712.4	13 700.1
(0,13,1)Σ	15 992.3	15 984.7	16 114.8	16 105.9	14 096.7	14 085.0	14 253.2	14 241.6
(0,14,1)Π	16 644.9	16 635.4	16 769.7	16 759.9	14 626.7	14 616.1	14 785.8	14 771.3
(0,15,1)Σ	17 295.8	17 288.0	17 429.1	17 419.6	15 147.1	15 134.4	15 325.8	15 313.1
(0,16,1)Π	17 955.1	17 947.7	18 087.8	18 079.0	15 667.6	15 653.0	15 858.2	15 843.9
(0,17,1)Σ	18 588.7	18 579.9	18 735.6	18 725.6	16 194.5	16 180.7	16 395.7	16 381.8
(0,18,1)Π	19 228.4	19 213.6	19 387.7	19 375.2	16 712.1	16 696.0	16 938.7	16 917.8
(0,19,1)Σ	19 873.8	19 864.1	20 033.6	20 023.1	17 238.4	17 223.4	17 462.2	17 447.1
(0,20,1)Π	20 507.2	20 499.9	20 675.5	20 664.7	17 754.0	17 742.8	17 988.4	17 971.9
(0,21,1)Σ	21 150.0	21 143.1	21 322.4	21 311.4	18 278.3	18 262.1	18 524.7	18 508.4
(0,1,2)Σ	8 939.6	8 926.7	9 008.1	8 995.7	8 639.7	8 627.1	8 696.3	8 684.2
(0,2,2)Π	9 613.1	9 595.4	9 691.3	9 687.6	9 124.7	9 116.3	9 208.9	9 200.1
(0,3,2)Σ	10 275.3	10 262.1	10 356.5	10 343.8	9 682.0	9 669.0	9 754.6	9 742.2
(0,4,2)Π	10 899.1	10 885.6	10 992.0	10 978.6	10 179.3	10 161.7	10 267.8	10 251.7
(0,5,2)Σ	11 606.0	11 592.4	11 700.1	11 687.0	10 727.1	10 713.7	10 817.2	10 804.3
(0,6,2)Π	12 255.9	12 245.0	12 351.5	12 341.7	11 221.7	11 212.1	11 326.9	11 334.1
(0,7,2)Σ	12 930.9	12 917.0	13 038.0	13 024.5	11 773.4	11 759.3	11 882.0	11 868.5
(0,8,2)Π	13 574.5	13 563.2	13 692.5	13 679.1	12 280.5	12 268.3	12 401.5	12 383.4
(0,9,2)Σ	14 249.4	14 235.1	14 369.2	14 355.3	12 819.7	12 804.9	12 947.4	12 933.2
(0,10,2)Π	14 893.4	14 876.4	15 022.4	15 007.2	13 339.9	13 331.8	13 453.1	13 449.2
(0,11,2)Σ	15 560.6	15 545.9	15 691.9	15 677.8	13 864.9	13 849.4	14 012.4	13 997.4
(0,12,2)Π	16 208.2	16 191.9	16 347.4	16 333.6	14 389.5	14 371.6	14 531.7	14 518.6
(0,13,2)Σ	16 879.7	16 864.6	17 018.4	17 003.7	14 908.3	14 892.0	15 076.1	15 060.3
(0,14,2)Π	17 530.3	17 506.5	17 676.9	17 658.2	15 425.7	15 398.9	15 591.8	15 571.7
(0,15,2)Σ	18 172.8	18 157.0	18 324.7	18 309.4	15 949.3	15 932.0	16 137.7	16 120.9

TABLE III. (*Continued.*)

(v_1, v_2, v_3)	$H^{11}B^{35}Cl$	$H^{11}B^{37}Cl$	$H^{10}B^{35}Cl$	$H^{10}B^{37}Cl$	$D^{11}B^{35}Cl$	$D^{11}B^{37}Cl$	$D^{10}B^{35}Cl$	$D^{10}B^{37}Cl$
(0,16,2)Π	18 797.0	18 783.6	18 953.8	18 942.8	16 453.1	16 434.6	16 659.0	16 647.6
(0,17,2)Σ	19 457.7	19 440.8	19 624.7	19 609.0	16 987.3	16 969.7	17 196.6	17 178.8
(0,18,2)Π	20 099.9	20 079.9	20 268.5	20 252.7	17 498.7	17 480.0	17 721.4	17 703.1
(0,19,2)Σ	20 736.6	20 719.4	20 916.2	20 900.1	18 021.6	18 002.5	18 252.2	18 233.4
(0,20,2)Π	21 376.3	21 366.1	21 560.1	21 542.0	18 544.1	18 520.8	18 765.5	18 744.4

to linearity of the ground state was calculated to be 6073 cm^{-1}, quite a bit lower than the 10 084 cm^{-1} value found for HBF.[11]

Using the Molpro code, the geometry independent phenomenological spin-orbit splitting of the electronic Π ($\tilde{X}^2A'$, $\tilde{A}^2A''$) state at its equilibrium geometry was calculated to be 87.3 cm^{-1}, at the complete active space self-consistent field (CASSCF) level of theory using the same basis set. This value is substantially larger than that calculated for HBF (42.3 cm^{-1})[11] but comparable in magnitude to the −79.4 cm^{-1} spin-orbit coupling constant calculated for BCl^+ by Bruna and Grein.[28]

C. Calculation of the vibronic energy levels

The analytically fitted surfaces were used for the variational calculation of the rovibronic energy levels. Preliminary analyses were performed using the RVIB3 code developed by Carter and co-workers.[29] However in the course of these tests, a paper by Mitrushchenkov was published,[30] pointing out some numerical difficulties with the RVIB3 code and its underlying theory to handle cases with very large Renner-Teller coupling, such as those which often occur in linear-bent systems. These difficulties occur only in the calculation of levels with $K > 0$ (Π state, Δ state, etc.). We then resorted to using a previous version of the same program, based on a different definition of the basis set for the bending motion,[31] which has proved to work correctly for linear-bent systems.[32]

The variational basis set was built from 20 harmonic oscillators for the BH and BCl stretches and 104 Legendre polynomials for the bend of the two electronic states,

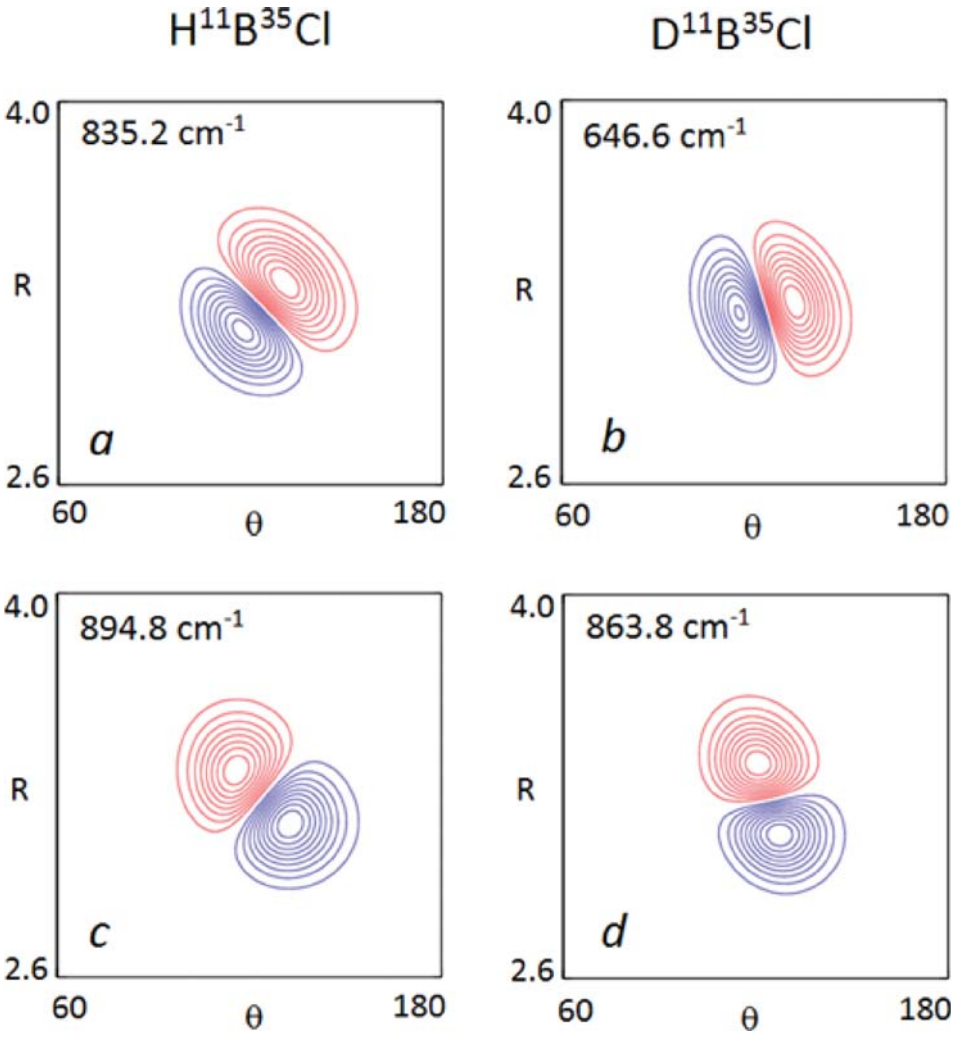

FIG. 2. Contour plots of the vibrational wavefunctions of $H^{11}B^{35}Cl$ and $D^{11}B^{35}Cl$ along the HBCl bending and BCl stretching coordinates (θ and R). The assignments for the two vibrational modes of DBCl are clearly (0,1,0) and (0,0,1) (panels (b) and (d)). The HBCl vibrational modes (panels (a) and (c)) were assigned based on their similarity to the vibrational wavefunctions of DBCl.

contracted to 51 two-dimensional stretching functions and 74 two dimensional bending functions. Spin-rovibronic calculations for $J = 1/2, 3/2, 5/2, 7/2$ were performed either with or without the inclusion of the spin-orbit effect, thus enabling the prediction of the energies and spin orbit splittings for levels with $K \leq 3$ (Σ, Π, Δ, and Φ levels). The vibrational quantum numbers were assigned by inspection of the variational coefficients and, for higher levels, by counting the nodes in plots of the vibrational wavefunctions. All eight isotopologues ($H^{11}B^{35}Cl$, $H^{10}B^{35}Cl$, $H^{11}B^{37}Cl$, $H^{10}B^{37}Cl$, $D^{11}B^{35}Cl$, $D^{10}B^{35}Cl$, $D^{11}B^{37}Cl$, and $D^{10}B^{37}Cl$) were studied, for energies up to 20 000 cm^{-1} above the $\tilde{X}^2A'$ (0,0,0) level.

The resulting calculated values for the low-lying ground state vibrational energy levels of the eight isotopologues of HBCl are given in Table II. In the ground electronic state of HBCl, there is an unusual mixing of the r_{BCl} stretching and θ_{HBCl} bending modes, which contribute with almost equal weight to the lowest two vibrational energy levels. This is clearly seen in Figure 2 (panels (a) and (c)). Such mixing makes the labeling of these two levels and their higher energy combinations ambiguous using the traditional ν_2 = bend and ν_3 = BCl stretch quantum numbers. To continue using them anyway, we made a comparison with the wavefunctions of the lowest two levels of the deuterated isotopologues (see Fig. 2, panels (b) and (d)), for which mode mixing is much less relevant. This comparison led us to assign the lowest energy level of HBCl as ν_2 and the second as ν_3. Overtone and combination levels have been then labeled accordingly. Table III shows the calculated (0,ν_2,0), (0,ν_2,1), and (0,ν_2,2) excited state energy levels, relative to the lowest ground state rovibronic energy level.

IV. EXPERIMENTAL RESULTS AND ANALYSIS

A. LIF spectra

The top panel of Fig. 3 shows a 2500 cm^{-1} portion of the total LIF spectrum of HBCl, obtained by monitoring total fluorescence through a long pass filter. In addition to bands of HBCl proven by recording single vibronic level emission spectra (*vide infra*), this spectrum contains many extraneous features due to other species produced in the discharge. The bottom trace shows the sync-scan LIF spectrum obtained by monitoring emission down to a level 835 ± 5 cm^{-1} to the red of the laser wavelength, corresponding to the nominal HBCl bending fundamental of $H^{11}BCl$, as shown in Table II. The corresponding level of $H^{10}BCl$ (~4 times less abundant) is ~10 cm^{-1} to higher energy (Table II) so the fluorescence of this isotopologue (and much of the impurity emission) is filtered out by the monochromator, greatly simplifying the spectrum.

Fig. 4 shows that a judicious choice of sync-scan offset, which depends on relative band intensities and Franck-Condon factors, can be used to completely separate the LIF spectra of $H^{11}BCl$ (offset = v_2'' fundamental) and $H^{10}BCl$ (offset = v_3'' fundamental) over an extensive spectral region. In each case, an extended bending progression is observed, and assignments can be made by comparison with theory as will be discussed later. In addition, the inset to the top trace of Fig. 4 illustrates that the chlorine isotope splittings are partially resolved in the spectra and considerations of relative intensities and calculated isotope shifts allow them to be assigned with confidence. The observed DBCl spectra were weaker and the ground state bending frequencies of the boron isotopologues are much closer in energy (Table II) so it was more difficult to resolve and assign the less abundant isotopologues although an extensive spectrum of $D^{11}B^{35}Cl$ was measured.

B. Emission spectra

SVL emission spectra of $H^{11}BCl$, $H^{10}BCl$, and $D^{11}BCl$ were measured in order to establish the ground state vibrational energy levels and for use in determining the upper state level symmetry (Σ or Π), a consequence of the operative $\Delta K = \pm 1$ selection rule. For example, Fig. 5 shows two $H^{11}BCl$ emission spectra. In the top trace, each emission band consists of a

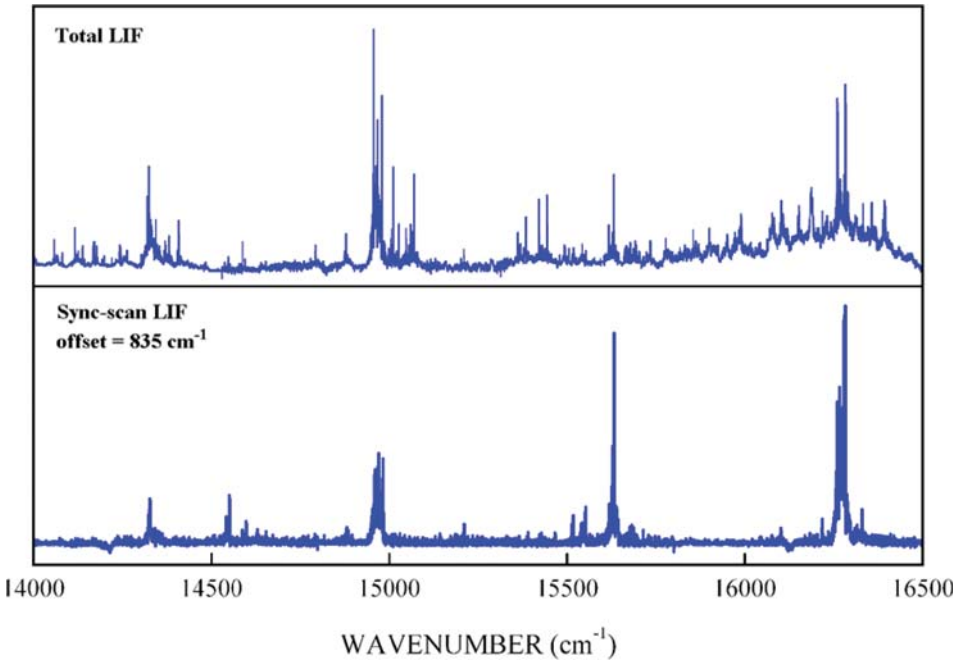

FIG. 3. Portions of the low-resolution total LIF spectra of HBCl (top) and the corresponding sync-scan LIF spectrum (bottom). The total LIF spectrum is overlapped with emission bands from impurities produced along with HBCl in the discharge. The sync-scan spectrum was recorded with a monochromator offset of 835 cm^{-1}, corresponding to the ground state HBCl bending fundamental of $H^{11}B^{35}Cl$.

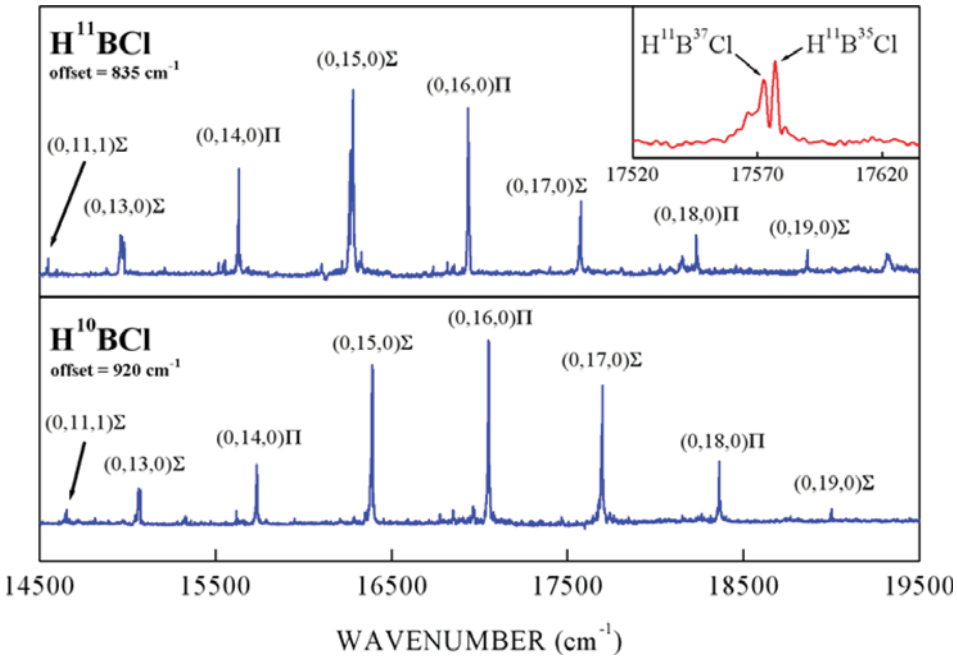

FIG. 4. Portions of the low-resolution sync-scan LIF spectra of $H^{11}BCl$ (top) and $H^{10}BCl$ (bottom) with upper state vibrational assignments. The inset shows that the bands of the two different chlorine Cl isotopologues can be resolved in these spectra.

single subband which must mean that the emission is from a $K = 0$ or Σ level which can only emit down to $K = 1$ in a lower state vibrational level. In contrast, the lower trace shows an emission spectrum in which each band has two features, separated by about 81 cm^{-1}. This splitting corresponds to approximately $4(A-(B+C)/2) \approx 78$ cm^{-1} from the data in Table I, and must therefore be the interval between $K = 2$ and $K = 0$ of the ground state asymmetric top. This proves that the upper state is a $K = 1$ or Π level. In this fashion, all the upper state symmetries for the transitions in Fig. 4 were assigned. It is noteworthy that the symmetries alternate between Σ and Π across the major progression, indicating that the former have odd quanta and the latter have even quanta of the upper state bending quantum number, v_2' since $K = |l \pm 1|$ and the vibrational angular momentum quantum number $l = v_2, v_2-2, v_2-4, \ldots, 1$ or 0.

Table IV shows the observed ground state vibrational energy levels measured in this work. These transitions were fitted to a simple anharmonic expansion and the resulting constants are presented in Table V. These constants are of only limited value as they are determined from very small data sets, are uncorrected for anharmonicity in some cases, and are unlikely to be as accurate as the quoted statistical errors suggest.

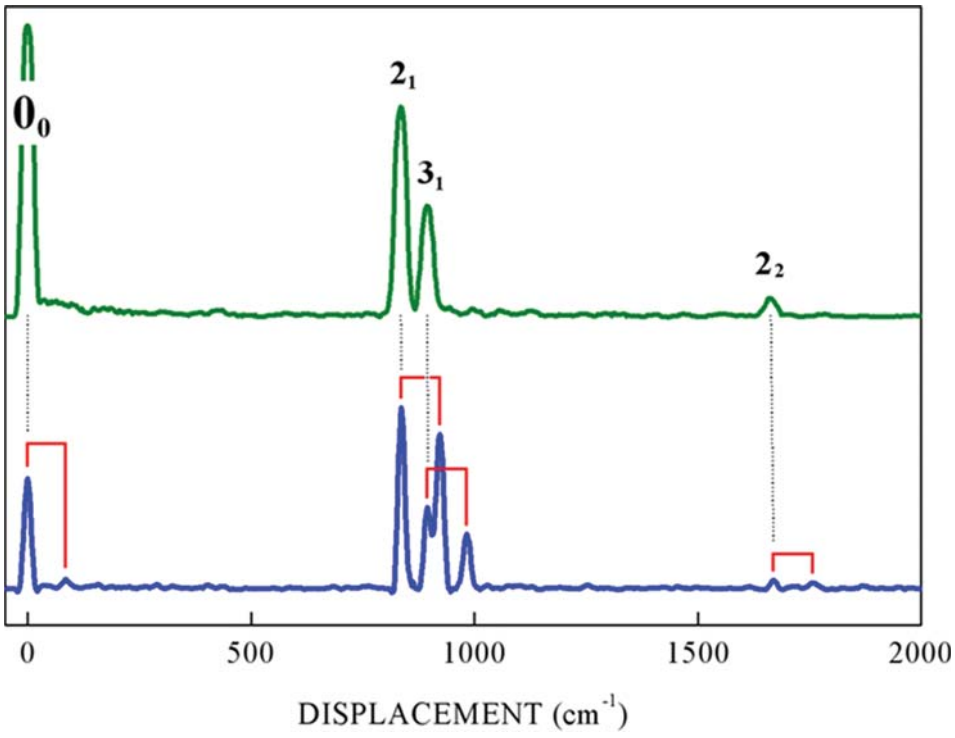

FIG. 5. Single vibronic level emission spectra of $H^{11}BCl$ with ground state vibrational assignments. The wavenumber scale is displacement from the excitation laser position which gives a direct energy measure of the ground vibrational energy. The upper trace was obtained by laser excitation of the (0,9,1) Σ level and the lower by populating the (0,10,1) Π state.

TABLE IV. Observed ground state energy levels (cm^{-1}), their assignments, and observed – calculated residuals from fitting to an anharmonic expansion from the emission spectra of $H^{11}BCl$, $D^{11}BCl$, and $H^{10}BCl$ isotopologues.

	$H^{11}BCl$		$D^{11}BCl$		$H^{10}BCl$	
Assignment	Energy[a]	Residual	Energy	Residual	Energy	Residual
3_1	895	−0.4	866	0.3	923	0.7
2_1	835	−0.4	646	−0.4	847	1.8
3_2	1776	−0.3	1722	−0.1	1830	−0.6
2_13_1	1722	1.4	1506	−0.3	1756	−0.3
2_2	1671	0.2	1291	1.1	1691	0.5
3_3	2643	0.1	…	…	…	…
1_1	2541	0.0	1908	0.8	…	…
2_13_2	…	…	2357	0.1	2654	0.6
2_23_1	2545	−0.7	2144	0.0	2590	−0.4
2_3	…	…	1930	−0.4	2535	−0.7
1_12_1	…	…	2549	−1.6	…	…
2_4	…	…	2568	−0.1	…	…
1_12_2	…	…	3192	0.8	…	…

[a]Energy above the lowest vibrational level of the $\tilde{X}^2A'$ state.

C. Assignment of the LIF spectra

By correlating the calculated transition frequencies (Table III), upper state symmetries, and isotope shifts with the observed progressions (Fig. 4), it is possible to obtain a consistent and reliable set of assignments for all the data. The results for HBCl are presented in Table VI. It is evident that there is a systematic offset between the observed and calculated transitions of $H^{11}B^{35}Cl$ of 100–145 cm^{-1} indicating that the excited state T_e is very slightly too high, very similar to the situation for HBF.[12] As shown in Table VI, the observed boron and chlorine isotope shifts for each band are in excellent agreement with the theoretical predictions. Other assignments, which would involve shifting the upper state by at least two quanta of the bending mode, due to the Σ, Π alteration, give an unreasonably large T_e error, and very poor isotope shift agreement. There is clearly only one set of assignments that bring theory and experiment into accord and all available tests indicate that they are correct.

The DBCl sync-scan LIF data and assignments are summarized in Table VII. These data show the same magnitude of difference between the observed and calculated band origins as found in Table VI. Unfortunately, the isotope data are not nearly as extensive in this case, due to weakness of the signals and our inability to obtain good sync-scan data for the less abundant isotopologues. Nevertheless, the theory is in excellent accord with the trends in the $D^{11}B^{35}Cl$ data, which involves three bending progressions, including 0, 1, and 2 quanta of the B–Cl stretch. As a further example, the highest observed bending level (0,19,0) has an H-D isotope shift of 2525.1 cm^{-1} and a calculated value of 2553.2 cm^{-1}, a discrepancy of only 1.1% at an energy of almost 19 000 cm^{-1} above the ground state. Such excellent agreement between theory and experiment strongly supports the validity of our analysis.

TABLE V. Ground state ($\tilde{X}^2A'$) vibrational constants (in cm^{-1}) of $H^{11}BCl$, $D^{11}BCl$, and $H^{10}BCl$.

Parameter	$H^{11}BCl$	$D^{11}BCl$	$H^{10}BCl$
ω_1^0	2541.0(10)	1907.18(99)	…
ω_2^0	835.40(45)	647.84(79)	845.25(31)
ω_3^0	902.6(11)	870.4(16)	929.3(16)
x_{12}^0	…	−2.93(85)	…
x_{22}^0	…	−1.45(23)	…
x_{23}^0	−10.23(77)	−5.81(63)	−11.18(62)
x_{33}^0	−7.21(42)	−4.67(79)	−6.99(84)

V. DISCUSSION

A. Molecular structure

Unfortunately, the weakness of the HBCl LIF signals and the overlapping bands of the two chlorine isotopologues precluded the acquisition of high resolution, rotationally resolved spectra from which molecular structures might be derived. We are then left with relying on the structures obtained from our *ab initio* calculations, at least until the microwave spectrum is observed (the B3LYP/aug-cc-pVTZ ground state dipole moment is 0.5 D). The best theoretical structures come from the potential surface calculations which yield r_{BH} = 1.190 Å, r_{BCl} = 1.716 Å, and θ = 123.4° for the bent ground state and r_{BH} = 1.166 Å and r_{BCl} = 1.681 Å for the linear excited state, very comparable to the optimized geometries in Table I. The ground state BH bond length is 0.013 Å shorter than the *ab initio* BH equilibrium bond length[11] of HBF but almost identical to the calculated value (1.188 Å)[33] for BH_2. This similarity is reflected in the BH stretching fundamentals; 2541 cm^{-1} (expt. Table IV) for HBCl and 2507 cm^{-1} (calc. Ref. 33) for BH_2. The calculated BCl bond length is identical to the ground state r_e = 1.715 Å of the BCl free radical,[34] and the BCl stretching ω_e values are also very similar (835.4 cm^{-1} for HBCl and 840.29 cm^{-1} for BCl). The HBCl ground state bond angle (123.4°) is intermediate between that of BH_2 (129.04°)[33] and HBF (121.1°),[11] suggesting that the angle is less a function of the size of the halogen than it is of the electronegativity.

TABLE VI. Observed $\tilde{A}^2A''\Pi - \tilde{X}^2A'$ transitions (cm^{-1}) of various HBCl isotopologues.

	$H^{11}B^{35}Cl$		$H^{11}B^{37}Cl$		$H^{10}B^{35}Cl$		$H^{10}B^{37}Cl$	
(ν_1, ν_2, ν_3)	Observed[a]	Observed − calculated[b]	Observed	Δ[c]	Observed	Δ	Observed	Δ
(0,8,0)Π	11 681.7	−113.8	11 679.2	0.5	11 745.4	−4.1	11 742.6	−3.4
(0,10,0)Π	13 001.2	−103.5	12 997.3	2.1	13 075.4	−1.6	13 073.6	−4.3
(0,12,0)Π	14 327.8	−113.4	14 324.6	0.4	14 412.2	4.9	14 408.5	4.2
(0,13,0)Σ	14 981.8	−109.5	…	…	15 072.1	2.8	15 069.0	2.6
(0,14,0)Π	15 632.3	−131.7	15 628.4	2.5	15 733.5	4.5	15 730.7	1.5
(0,15,0)Σ	16 281.6	−115.2	16 278.1	−0.5	16 390.0	0.4	16 386.2	0.4
(0,16,0)Π	16 937.6	−129.8	16 932.9	1.8	17 053.3	4.0	17 048.8	5.9
(0,17,0)Σ	17 577.2	−118.7	17 572.7	−0.2	17 700.0	0.1	17 695.5	0.2
(0,18,0)Π	18 231.5	−126.5	…	…	18 368.7	0.7	…	…
(0,19,0)Σ	18 863.5	−123.4	18 858.7	0.4	18 999.8	0.2	18 994.6	0.4
(0,9,1)Σ	13 236.8	−105.2	13 228.0	0.4	13 329.5	0.5	13 323.0	−1.1
(0,10,1)Π	13 896.6	−123.3	13 886.2	3.1	…	…	…	…
(0,11,1)Σ	14 550.2	−107.5	14 541.4	0.2	…	…	…	…
(0,12,1)Π	15 203.4	−127.2	…	…	…	…	…	…
(0,13,1)Σ	15 853.6	−119.3	15 844.8	1.2	…	…	…	…
(0,12,2)Π	16 101.0	−107.2	…	…	…	…	…	…
(0,13,2)Σ	16 739.0	−121.3	…	…	…	…	…	…
(0,14,2)Π	17 402.3	−128.0	…	…	…	…	…	…
(0,15,2)Σ	18 029.1	−124.3	…	…	…	…	…	…

[a]The Q-branch maxima of each band.
[b]The calculated values are taken from our theoretical study listed in Table III. The calculated Σ band origins were corrected by subtracting the $K_a = 1$ level of the (0,0,0) ground state.
[c]The values are observed – calculated isotope shifts.

TABLE VII. Observed $\tilde{A}^2A''\Pi - \tilde{X}^2A'$ transitions (cm^{-1}) of various DBCl isotopologues.

	$D^{11}B^{35}Cl$		$D^{11}B^{37}Cl$		$D^{10}B^{35}Cl$	
(ν_1, ν_2, ν_3)	Observed[a]	Observed − calculated[b]	Observed	Δ[c]	Observed	Δ
(0,13,0)Σ	13 169.3	−101.2	13 162.4	−0.1	…	…
(0,14,0)Π	13 703.2	−100.6	…	…	…	…
(0,15,0)Σ	14 229.4	−101.5	14 220.2	0.9	…	…
(0,16,0)Π	14 766.8	−104.0	…	…	…	…
(0,17,0)Σ	15 285.2	−103.1	15 275.9	−0.3	15 477.4	1.3
(0,18,0)Π	15 819.1	−105.2	15 808.0	−0.3	…	…
(0,19,0)Σ	16 338.4	−103.6	16 327.2	0.3	16 556.9	−1.0
(0,20,0)Π	16 873.1	−114.7	…	…	…	…
(0,11,1)Σ	12 934.3	−98.4	…	…	…	…
(0,12,1)Π	13 461.2	−108.2	…	…	…	…
(0,13,1)Σ	13 984.6	−101.0	…	…	…	…
(0,14,1)Π	14 523.5	−103.2	…	…	…	…
(0,15,1)Σ	15 036.0	−100.0	…	…	…	…
(0,16,1)Π	15 569.5	−98.1	…	…	…	…
(0,17,1)Σ	16 082.4	−101.0	16 068.2	0.4	16 283.9	−0.6
(0,18,1)Π	16 607.1	−105.0	16 594.8	−3.8	…	…
(0,19,1)Σ	17 122.2	−105.1	…	…	…	…
(0,9,2)Σ	12 713.7	−94.9	…	…	…	…
(0,10,2)Π	13 237.1	−102.8	…	…	…	…
(0,11,2)Σ	13 756.9	−96.9	…	…	…	…
(0,12,2)Π	14 282.8	−106.7	…	…	…	…
(0,13,2)Σ	14 800.1	−97.1	…	…	…	…
(0,14,2)Π	15 323.9	−101.8	…	…	…	…
(0,15,2)Σ	15 838.2	−100.0	15 821.3	−0.3	16 027.9	−1.6

[a]The Q-branch maxima of each band.
[b]The calculated values are taken from our theoretical study listed in Table III. The calculated Σ band origins were corrected by subtracting the $K_a = 1$ level of the (0,0,0) ground state.
[c]The values are observed − calculated isotope shifts.

On electronic excitation, the molecule adopts a linear conformation, in accord with the predictions of Walsh diagrams for 11 valence electron HAB systems. Both bond lengths decrease ($\Delta r_{BH} = -0.024$ Å and $\Delta r_{BCl} = -0.035$ Å) on going from the ground to the excited state, similar to the trends found for BH_2 ($\Delta r_{BH} = -0.018$ Å)[33] and HBF ($\Delta r_{BH} = -0.036$ Å and $\Delta r_{BF} = -0.002$ Å).[11] The calculated barrier to linearity ($\tilde{A} - \tilde{X}$ state energy difference) varies dramatically with the halogen substituent, from a very small 2743 cm^{-1} for BH_2,[33] and a moderate 6073 cm^{-1} for HBCl, to a very large 10 099 cm^{-1} value for HBF.[11]

B. Comparison between theory and experiment

The agreement between the observed (Table IV) and calculated (Table II) ground state energy levels of HBCl and DBCl is excellent. The bending and BCl stretching fundamentals are calculated to within experimental error (±2 cm^{-1}) and the calculated higher frequency BH stretches differ from experiment by 3.2 ($H^{11}BCl$) and 8.6 cm^{-1} ($D^{11}BCl$). The agreement is of similar quality for the limited number of observed overtone and combination levels. It is clear that the calculated ground state potential energy surface provides a good description of the low-lying vibrational energy levels.

Theory predicts that the $\tilde{A} - \tilde{X}$ electronic transition of HBCl involves a change from a bent ground state structure to a linear excited state geometry and this should give rise to an extensive band system with pronounced activity in the bending mode. The data and assignments in Tables VI and VII and Fig. 4 show that this is precisely what is observed. The experimentally validated alternation between Σ and Π bands in the pure bending progression confirms the linear-bent nature of the transition.

As previously noted, the theoretically predicted excited state energy levels are approximately 100 cm^{-1} higher than their experimentally measured counterparts. This implies that a very small (~1.6%) downward correction in the barrier to linearity would bring theory and experiment into excellent agreement. It is very gratifying that theory does such a good job at predicting the excited state energy levels as it would be very difficult to reliably assign the spectrum without it.

VI. CONCLUSIONS

Using the sync-scan LIF method, we have obtained extensive vibrationally resolved electronic spectra in the 860–525 nm region that can be definitively attributed to the $\tilde{A}^2A''\Pi - \tilde{X}^2A'$ band systems of the HBCl and DBCl free radicals. Single vibronic level emission spectra were analyzed to establish the ground state vibrational energy levels and the upper state Σ or Π vibronic symmetry. High level *ab initio* theory was used to calculate the ground and excited state potential energy surfaces and the energy levels were determined variationally. These theoretical results were found to correlate very well with the experimental observations, allowing us to make a complete set of assignments for the observed bands. The spectrum arises from an electronic transition between the two components of an orbitally degenerate $^2\Pi$ state which is split by a strong vibronic interaction producing a bent ground state and a linear excited state.

ACKNOWLEDGMENTS

The research of the Clouthier group was supported by the National Science Foundation. R.T. acknowledges financial support from the University of Bologna.

[1]O. Sezer and J. I. Brand, Mater. Sci. Eng. B **79**, 191 (2001).
[2]S. Le Gallet, G. Chollon, F. Rebillat, A. Guette, X. Bourrat, R. Naslain, M. Couzi, and J. L. Bruneel, J. Eur. Ceram. Soc. **24**, 33 (2004).
[3]N. A. Sezgi, T. Dogu, and H. O. Ozbelge, Chem. Eng. Sci. **54**, 3297 (1999).
[4]N. A. Sezgi, A. Ersoy, T. Dogu, and H. O. Ozbelge, Chem. Eng. Process. **40**, 525 (2001).
[5]J. Berjonneau, G. Chollon, and F. Langlais, J. Electrochem. Soc. **153**, C795 (2006).
[6]H. B. Schlegel and S. J. Harris, J. Phys. Chem. **98**, 11178 (1994).
[7]H. B. Schlegel, A. G. Baboul, and S. J. Harris, J. Phys. Chem. **100**, 9774 (1996).
[8]M. D. Allendorf and C. F. Melius, J. Phys. Chem. A **101**, 2670 (1997).
[9]S. J. Harris, J. Kiefer, Q. Zhang, A. Schoene, and K.-W. Lee, J. Electrochem. Soc. **145**, 3203 (1998).
[10]S.-G. He, F. X. Sunahori, and D. J. Clouthier, J. Am. Chem. Soc. **127**, 10814 (2005).
[11]F. X. Sunahori, D. J. Clouthier, S. Carter, and R. Tarroni, J. Chem. Phys. **130**, 164309 (2009).
[12]F. X. Sunahori and D. J. Clouthier, J. Chem. Phys. **130**, 164310 (2009).
[13]H. Harjanto, W. W. Harper, and D. J. Clouthier, J. Chem. Phys. **105**, 10189 (1996).
[14]D. L. Michalopoulos, M. E. Geusic, P. R. R. Langridge-Smith, and R. E. Smalley, J. Chem. Phys. **80**, 3556 (1984).
[15]J. Yang and D. J. Clouthier, J. Chem. Phys. **135**, 054309 (2011).
[16]M. J. Frisch, G. W. Trucks, H. B. Schlegel *et al.*, Gaussian 03, Revision C.02 (Gaussian, Inc., Wallingford, CT, 2004).
[17]T. H. Dunning, Jr., J. Chem. Phys. **90**, 1007 (1989).
[18]K. Dressler and D. A. Ramsey, Philos. Trans. R. Soc., A **251**, 553 (1959).
[19]G. Herzberg and J. W. C. Johns, Proc. R. Soc. A **298**, 142 (1967).
[20]J. W. C. Johns, S. H. Priddle, and D. A. Ramsay, Discuss. Faraday Soc. **35**, 90 (1963).
[21]H. Lew, Can. J. Phys. **54**, 2028 (1976).
[22]J. F. Stanton, J. Gauss, M. E. Harding, and P. G. Szalay, CFOUR, A Quantum-Chemical Program Package, with contributions from A. A. Auer, R. J. Bartlett, U. Benedikt, C. Berger, D. E. Bernholdt, Y. J. Bomble, L. Cheng, O. Christiansen, M. Heckert, O. Heun, C. Huber, T.-C. Jagau, D. Jonsson, J. Jusélius, K. Klein, W. J. Lauderdale, D. A. Matthews, T. Metzroth, L. A. Mück, D. P. O'Neill, D. R. Price, E. Prochnow, C. Puzzarini, K. Ruud, F. Schiffmann, W. Schwalbach, S. Stopkowicz, A. Tajti, J. Vázquez, F. Wang, and J. D. Watts; *Integral packages MOLECULE* (J. Almlöf and P. R. Taylor), *PROPS* (P. R. Taylor), *ABACUS* (T. Helgaker, H. J. A. Jensen, P. Jørgensen, and J. Olsen), and *ECP routines* (A. V. Mitin and C. van Wüllen). For the current version, see http://www.cfour.de.
[23]H.-J. Werner, P. J. Knowles, G. Knizia, F. R. Manby, M. Schütz *et al.*, MOLPRO, version 2010.1, a package of *ab initio* programs, 2010, see http://www.molpro.net.
[24]K. Raghavachari, G. W. Trucks, J. A. Pople, and M. Head-Gordon, Chem. Phys. Lett. **157**, 479 (1989).
[25]R. A. Kendall, T. H. Dunning, Jr., and R. J. Harrison, J. Chem. Phys. **96**, 6796 (1992); D. E. Woon and T. H. Dunning, Jr., *ibid.* **103**, 4572 (1995); T. H. Dunning, Jr., K. A. Peterson, and A. K. Wilson, *ibid.* **114**, 9244 (2001).
[26]J. Senekowitsch, Ph.D. thesis, Johann Wolfgang Goethe Universität, Frankfurt am Main, Germany, 1988.
[27]See supplementary material at http://dx.doi.org/10.1063/1.4904892 for a table of the expansion coefficients of the HBCl potential energy surfaces.
[28]P. J. Bruna and F. Grein, J. Phys. Chem. A **105**, 3328 (2001).
[29]S. Carter, N. C. Handy, C. Puzzarini, R. Tarroni, and P. Palmieri, Mol. Phys. **98**, 1697 (2000).
[30]A. O. Mitrushchenkov, J. Chem. Phys. **136**, 024108 (2012).
[31]S. Carter, N. C. Handy, P. Rosmus, and G. Chambaud, Mol. Phys. **71**, 605 (1990).
[32]M. Brommer, B. Weis, B. Follmeg, P. Rosmus, S. Carter, N. C. Handy, H. J. Werner, and P. J. Knowles, J. Chem. Phys. **98**, 5222 (1993).
[33]M. Kolbuszewski, P. R. Bunker, W. P. Kraemer, G. Osmann, and P. Jensen, Mol. Phys. **88**, 105 (1996).
[34]A. G. Maki, F. J. Lovas, and R. D. Suenram, J. Mol. Spectrosc. **91**, 424 (1982).